Clinical Radiology 73 (2018) 975–980

Contents lists available at ScienceDirect

Clinical Radiology

journal homepage: www.clinicalradiologyonline.net

Efficacy of 3D VIBE Dixon fat quantification for differentiating clear-cell from non-clear-cell renal cell carcinoma

S.-r. Li [a], M.H. Pui [b], Y. Guo [a,*], H.-j Wang [a], J. Guan [a], X.-l. Zhang [a], W.-b. Pan [a]

[a] Department of Radiology, The First Affiliated Hospital of Sun Yat-sen University, 58 Zhongshan Road 2, Guangzhou, Guangdong, People's Republic of China
[b] Department of Radiology, Timmins District Hospital, 700 Ross Avenue E, Timmins, Ontario P4N 8P2, Canada

ARTICLE INFORMATION

Article history:
Received 26 May 2017
Accepted 27 June 2018

AIM: To assess the efficacy of three-dimensional (3D) volumetric interpolated breath-hold examination (VIBE) magnetic resonance imaging (MRI) with Dixon quantification for differentiating clear-cell from non-clear-cell types of renal cell carcinoma (RCC).

MATERIALS AND METHODS: The 3D VIBE Dixon renal MRI examinations of 44 patients with 45 histologically confirmed RCCs was analysed. The fat fractions and signal intensity indexes (SI_{index}) of the solid portions of clear-cell and non-clear-cell RCCs were measured and compared using Student's *t*-test and receiver operating characteristic (ROC) curves. The agreement of measurements among observers was evaluated by the intraclass correlation coefficient (ICC), and Bland–Altman plots.

RESULTS: The mean values of fat fraction (13.16±7.16%) and SI_{index} (22.64±15.7%) in clear-cell RCCs were significantly higher than that in non-clear-cell RCCs (7.7±2% and 7.9±4.8%; $p<0.001$, respectively). With the area under the ROC curve (AUC) of the fat fraction at 0.811, 75% (95% CI: 55.1–89.43%) sensitivity and 76.5% (95% CI: 50.1–93.2%) specificity for diagnosing clear-cell RCC were obtained at a cut-off fat fraction value of 8.9%. With a cut-off value of 8.89%, the diagnostic sensitivity and specificity were 85.7% (95% CI: 67.3–96%) and 70.6% (95% CI: 44–89.7%), respectively. The AUC of the SI_{index} was 0.870 (0.766–0.973). ICC and Bland–Altman plots show excellent agreement of the tumour fat fraction and SI_{index} measurement between the two observers.

CONCLUSION: Intracellular lipid content analysis using the 3D Dixon technique can help to differentiate clear-cell from non-clear-cell RCCs.

© 2018 The Royal College of Radiologists. Published by Elsevier Ltd. All rights reserved.

Introduction

Clear-cell renal cell carcinoma (RCC) is the most common histological subtype accounting for 65–80% of all RCCs. Non-clear-cell RCC includes papillary (10–15%), chromophobe (4–5%), collecting duct (1–2%), and other rare or

* Guarantor and correspondent: Y. Guo, Department of Radiology, The First Affiliated Hospital of Sun Yat-sen University, 58 Zhongshan Road 2, Guangzhou, Guangdong, People's Republic of China. Tel.: +86(20) 87755766, extn: 8471; fax: +86(20) 87615805.
E-mail address: dr.guoyan@163.com (Y. Guo).

https://doi.org/10.1016/j.crad.2018.06.018
0009-9260/© 2018 The Royal College of Radiologists. Published by Elsevier Ltd. All rights reserved.

unclassified (4–5%) subtypes.[1,2] Each subtype of RCC is associated with a different prognosis. Compared with common types of non-clear-cell RCC, such as papillary RCC and chromophobe RCC, clear-cell RCC have an unfavourable prognosis, with a 5-year survival rate of 44–69%, and it accounts for 94% of metastatic RCC.[3] Differentiating clear-cell from non-clear-cell subtypes is crucial for prognosis assessment and treatment management. Clear-cell RCC typically presents as a heterogeneous hyper-vascular mass with a variable amount of intracellular lipid. Magnetic resonance imaging (MRI) signal intensities (SIs) and contrast enhancement patterns, apparent diffusion coefficient values on diffusion-weighted imaging (DWI), and the presence of macro- or microscopic fat on chemical shift imaging (CSI) have been used to differentiate clear-cell from non-clear-cell RCC.[4–8] Previous investigators have reported conflicting results of detecting or quantifying intracellular lipid on CSI for differentiating subtypes of RCC. Clear-cell RCC was reported to exhibit a decrease in SI on out-of-phase compared with in-phase CSI because of its intracellular lipid content.[6] Other studies showed that non-clear-cell RCC also demonstrated SI drop on out-of-phase CSI.[9,10] These observations were based on quality analysis or calculation of the SI index (SI_{index}); however, qualitative analysis of focal or diffuse SI drop on out-of-phase CSI showed no significant association with histology.[9,11,12] The objective of this study was to assess the value of three-dimensional (3D) volumetric interpolated breath-hold examination (VIBE) MRI sequences with Dixon quantification of intracytoplasmic lipid for differentiating clear-cell from non-clear-cell RCCs.

Materials and methods

The study was conducted in accordance with ethical guidelines for human research, the Health Insurance Portability and Accountability Act and was approved by the institutional research ethics committee. Written informed consent was obtained from all patients. From November 2014 through September 2017, consecutive patients with suspected RCC on ultrasound or computed tomography (CT) who underwent renal MRI before treatment at The First Affiliated Hospital of Sun Yat-sen University were enrolled in the study. Patients with other renal pathology or no histology confirmation were excluded. All renal MRI examinations were performed on a 3 T MRI system (Magnetom Trio, Siemens Medical Solutions, Erlangen, Germany) with an eight-channel phased-array coil. Axial and coronal 3D T1-weighted VIBE Dixon images (5.5 ms repetition time [TR], 2.5 ms echo time 1 [TE1], 3.7 ms TE2, 10° flip angle, 504 Hz/pixel bandwidth, 1 echo train length, 32–40 cm field-of-view [FOV], 320×240 matrix, 2 mm section thickness) and two-dimensional (2D) T2-weighted (W) periodically rotated overlapping parallel lines with enhanced reconstruction (BLADE) images (3,875 ms TR, 78 ms TE, 140° flip angle, 240 Hz/pixel bandwidth, 9 echo train length, 32–40 cm FOV, 320×240 matrix, 5 mm section thickness) of the kidneys were obtained. Axial and coronal 3D T1-weighted VIBE sequences (4.37 ms TR, 1.45 ms TE, 13° matrix, 210 Hz/pixel bandwidth, 1 echo train length, 32–40 cm FOV, 384×204 matrix, 5 mm section thickness) were then acquired at 5 seconds, 50 seconds, 2 minutes, and 4 minutes after intravenously injecting 0.1 mmol/kg body weight of Gd-DTPA (Magnevist, Bayer-Schering Pharma, Berlin, Germany) at 3 ml/s followed by 15 ml of normal saline flush using a power injector (EmpowerMR, ACIST Medical Systems, Eden Prairie, Minnesota, USA).

In the present study, only the Dixon images and the fat content maps were evaluated. Other images, such as T2W imaging and contrast-enhanced images, were referred to when necessary, but were not specifically analysed for the purpose of this study.

Lesion size, defined as the largest dimension on axial T2W images, was measured by one radiologist with 5 years of MRI experience. None of the tumours contained macroscopic fat. The 3D T1W VIBE Dixon sequence produced in-phase, out-of-phase, fat-only (SI_{fat}), and water-only (SI_{water}) images. Fat content maps were generated by an image-processing program, ImageJ (Version 1.51s, National Institutes of Health, Bethesda, Maryland, USA) according to the following algorithm:

$$\text{Fat fraction} = SI_{fat}/(SI_{water}+SI_{fat}).$$

The quality of the images were analysed, and it was determined whether the images were acceptable for further analysis or not. Those with lesion size <1 cm, with poor image quality or were composed mainly of cystic or necrosis areas were excluded from the study. Two experienced abdominal radiologists (reader 1 with 10 years of experience; reader 2 with 5 years of experience) independently defined the regions of interest (ROIs) without knowledge of the pathology results.

The measurement results were averaged between the two readers for further analyses. The axial or coronal 3D T1-weighted VIBE Dixon images, fat content maps and 3D T1-weighted contrast enhanced images were displayed simultaneously and ROIs were drawn to encompass most of the solid tumour without cystic degeneration, necrosis, or haemorrhage by another radiologist with 10 years of abdominal MRI experience without knowledge of the pathology results (Fig 1). The axial plane was first observed and assessed. If image quality or the depiction of the lesion were not satisfactory, the coronal plane was then observed and assessed. The five ROIs were drawn in five axial planes or five coronal planes. The interval between planes was approximately 20%. That is to say, the five planes were located approximately at the 10%, 30%, 50%, 70%, and 90% thickness of the tumour. A freehand ROI was defined on the in-phase or out-of-phase images, T2WI and post-contrast images were referred to for verification of the solid portion of the tumours and lesion boundaries. The ROI was then defined and added in “ROI Manager”, where ROIs can be stored. The ROIs than applied to the corresponding Dixon images and fat content maps. Care was taken to exclude cystic or necrotic areas from the ROIs, which was unenhanced after intravenous injection of contrast media. For each lesion, five ROIs from five axial or coronal slices of the

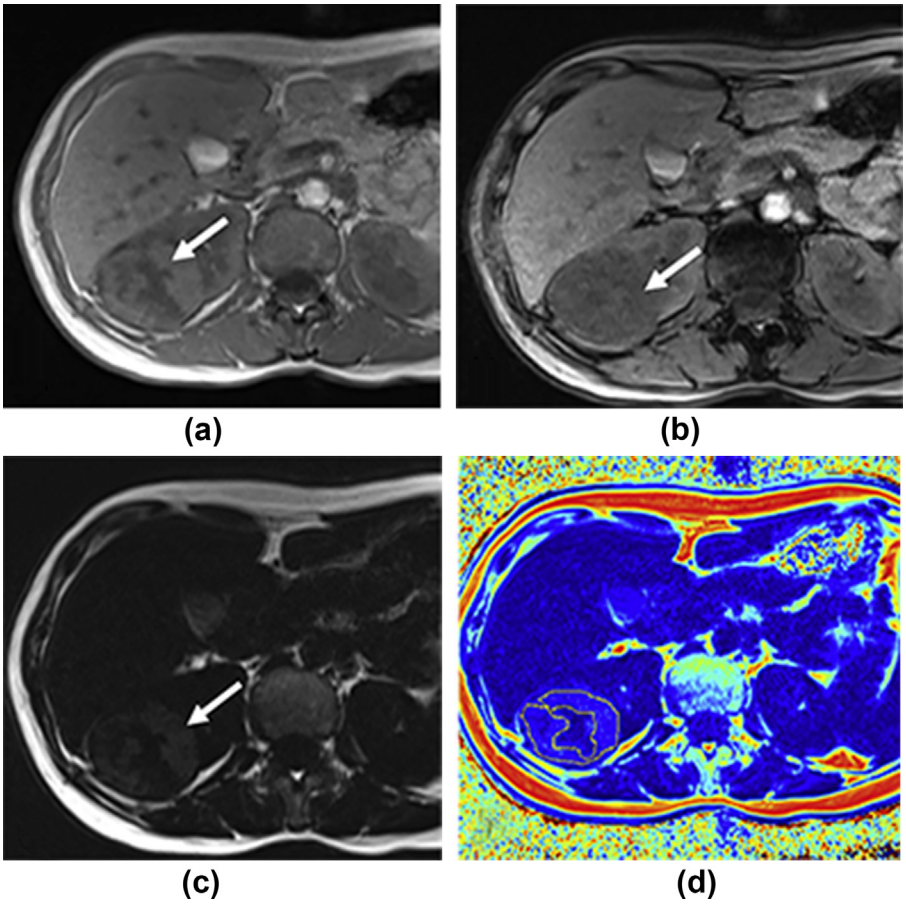

Figure 1 A 39-year-old woman with clear-cell RCC. The transverse in-phase image (a) shows solid tumour component (arrow) with marked decrease in signal intensity on the out-of-phase image (b). (c) On the fat-phase image, the solid component is hyper intense. (d) On the fat content map, the fat fraction of the yellow ROI is 14%.

tumour were selected and the average value was applied for analysis. The SI_{index} was calculated as:

$SI_{index} = (SIin\text{-}phase - SIout\text{-}of\text{-}phase)/SIin\text{-}phase$.[9]

Statistical analysis was performed using SPSS version 13.0 (Chicago, IL, USA) and MedCalc version 13. (MedCalc Software, Ostend, Belgium). The agreement of measurements among observers was evaluated by the intraclass correlation coefficient (ICC; where K <0.20 indicated poor; 0.21–0.40 fair, 0.41–0.60 moderate, 0.61–0.80 good, and 0.81–1.00 very good agreement), and Bland–Altman plots. For Bland–Altman plots, data are given as plots showing the absolute difference between corresponding measurements of both observers (*y*-axis) against the average of both observers (*x*-axis). The relative difference between measurements (absolute difference divided by the average) gives the bias; its standard deviation gives the random variation. The limits of agreement were calculated as mean bias±1.96 SD. The fat fraction and SI_{index} of clear-cell and non-clear-cell RCCs were graphically depicted as box-and-whisker plots and the average values were compared using Student's *t*-test. *p*-Values<0.05 were considered statistically significant. Receiver operating characteristic (ROC) curves were generated and the areas under the ROC curves (AUCs) were determined to select an optimal threshold for diagnosing clear-cell and non-clear-cell RCCs. To determine the cut-off point for each index, the Youden index (sensitivity+ specificity−1) was calculated and the corresponding cut-off value for the highest Youden index was considered as the optimal cut-off value.

Results

Of 112 patients who underwent MRI, 44 patients (29 men, 15 women; age range 18–80 years, mean 52.3 years) with 45 histologically confirmed RCCs after radical (27) and partial nephrectomy (17 cases) were included in the study. Patients with other renal pathology (22 cases, including six angiomyolipomas, one synovial sarcoma, one tumour with perivascular epithelioid cell differentiation, one epithelioid angiomyolipoma, one high-grade urothelial carcinoma of the renal pelvis, one well-differentiated liposarcoma, one adult nephroblastoma, one solitary fibrous tumour, one leiomyoma, one neurofibromatosis, one adult mesodermal kidney tumour, one renal eosinophiloma, one nephroblastoma, and four unspecified RCCs) or no histology confirmation (37 cases) were excluded from analysis. Nine cases were also excluded because of poor image quality

(three cases), small lesion size (two cases), or mainly cystic or necrosis areas (four cases). There were 28 clear-cell, 11 papillary and six chromophobe RCCs with one patient having two clear-cell RCCs in the same kidney. The size of clear-cell RCC (mean: 4.4 cm; range: 1–12.5 cm) and that of non-clear-cell RCC (mean: 4.1 cm; range: 1.2–10 cm) were with no statistically significance (p=0.64). In regards to intra-observer variability, the ICC for tumour fat fraction and SI_{index} measurement were excellent (0.986, 95% confidence Interval [CI] 0.975–0.992, and 0.990, 95% CI: 0.982–0.994 respectively). Bland–Altman plots show agreement of the tumour fat fraction and SI_{index} measurement between two observers. The 95% limits of agreement of tumour fat fraction measurement were −2.2 and 2.1% (mean difference, −0.1%; Fig 2a). The 95% limits of agreement of SI_{index} measurement were −4% and 4% (mean difference, 0; Fig 2b). The metrics all show excellent agreement between the two observers. The mean values of the fat fraction (13.16±7.16%) and SI_{index} (22.64±15.7%) in clear-cell RCC were significantly higher (p<0.001, respectively) than that in non-clear-cell RCC (7.7±2%, 7.9±4.8%; Fig 3). The cut-off value, estimated by the ROC curve at an optimal level of sensitivity and specificity, was 8.9% for fat fraction, with 75% (95% CI: 55.1–89.43%) sensitivity and 76.5% (95% CI: 50.1–93.2%) specificity. The AUC of the fat fraction was 0.811 (95% CI: 0.686–0.936; Fig 4). The cut-off value was 8.89% for the SI_{index}, with 85.7% (95% CI: 67.3–96%) sensitivity and 70.6% (95% CI: 44.–89.7%) specificity, respectively. The AUC of the SI_{index} was 0.870 (0.766–0.973; Fig 4). There were 15 small clear-cell RCCs and 10 small non-clear-cell RCCs, accounting for 55.6% of the total RCCs (25/45). For small renal masses that are <4 cm in maximal diameter, the mean values of the fat fraction (13.95±7.41%) and SI_{index} (21.23±15.87%) in clear-cell RCC were significantly higher than that in non-clear-cell RCC (7.84±2.46%, 8.61±4.30%, p=0.041, p=0.036, respectively). The cut-off value was 6.9% for the fat fraction, with 92.86% (95% CI: 66.1–99.8%) sensitivity and 63.64% (95% CI: 30.8–89.1%) specificity. The AUC of the fat fraction was 0.808 (95% CI: 0.603–0.937). The cut-off value was 13.85% for the SI_{index}, with 64.29% (95% CI: 35.1–87.2%) sensitivity and 90.91% (95% CI: 58.7–99.8%) specificity, respectively. The AUC of the SI_{index} was 0.851 (95% CI: 0.652–0.960).

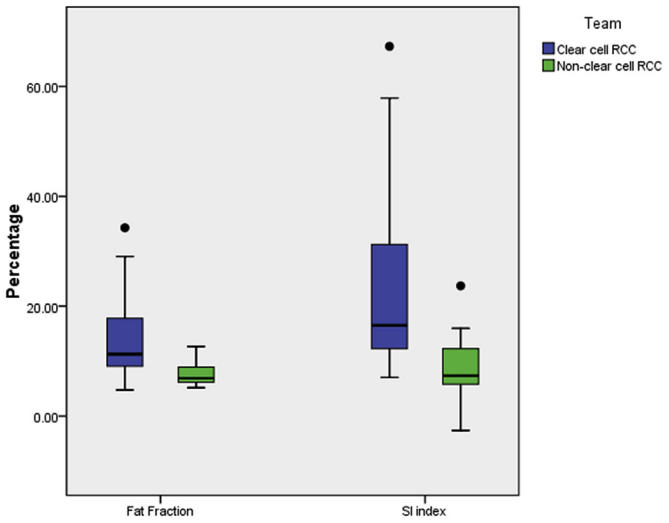

Figure 3 Box and whisker chart shows the ranges and mean values of the fat fraction and SI_{index} in clear-cell RCC and non-clear-cell RCC. Black dots represent outliers.

Discussion

Compared with common types of non-clear-cell RCC, such as papillary and chromophobe RCC, clear-cell RCC have an unfavourable prognosis, with a 5-year survival rate of 44–69%, and it accounts for 94% of metastatic RCC.[3] Pre-operative or pre-treatment accurate diagnosis has important clinical significance for clinical treatment plan and prognosis. MRI can be particularly helpful when renal lesions are detected but cannot be well characterised. Advantages of MRI include a lack of ionising radiation and superior soft-tissue contrast compared to CT. In addition, MRI has tremendous potential for multiparametric imaging. Its role in renal mass characterisation will likely continue to grow. In this study, the differentiation of clear-cell RCC from non-clear-cell RCC was based on the fat fraction and SI_{index} derived from 3D Dixon MRI.

Unlike MR spectroscopy, the Dixon technique provides in-phase, out-of-phase, fat-only, and water-only images with single breath-hold. It is easier to acquire and the image

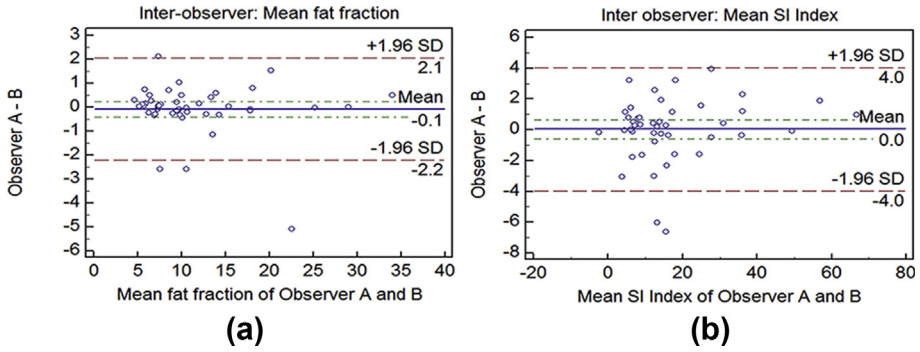

Figure 2 Bland–Altman plots show agreement of the tumour fat fraction and SI_{index} measurement between the two observers. The solid line in the graph represents the mean of the differences. The dotted line in the graph represents the corresponding 95% limits of agreement. The Bland–Altman plots demonstrated good consistency between the two observers.

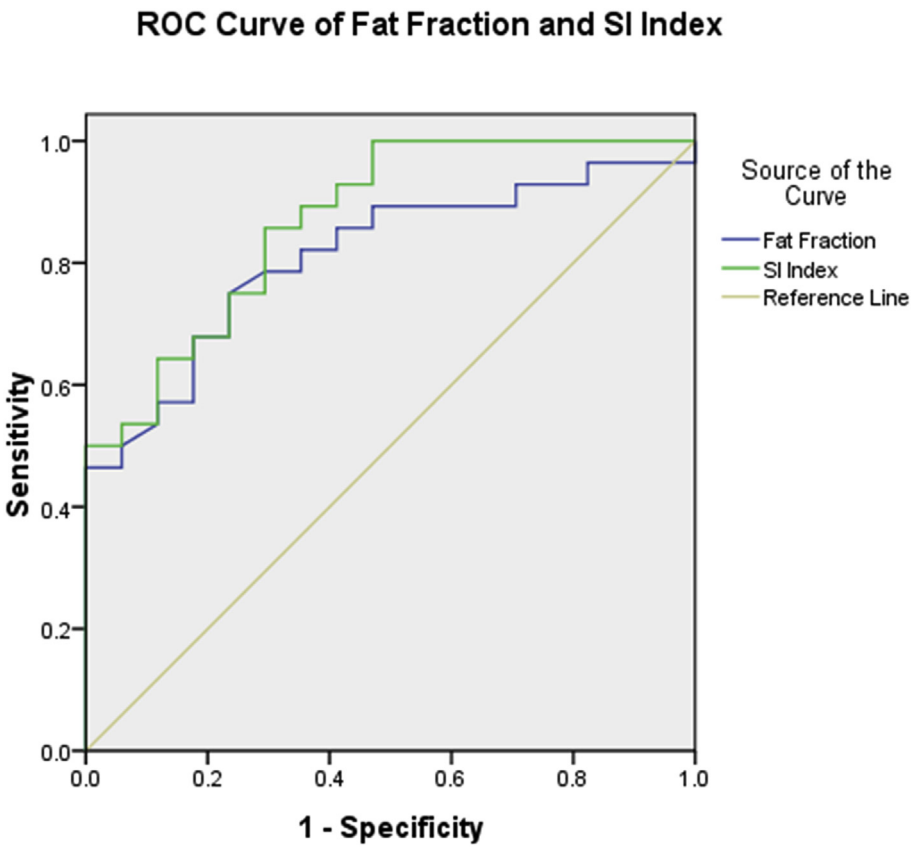

Figure 4 ROC curves of the fat fraction and SI_{index} for differentiating clear-cell RCC from non-clear-cell RCC.

analysis is also more straightforward. Lipid measurement in the liver and adrenal lesion using the Dixon technique has been reported.[13–15] To the authors' knowledge, this is the first application of the Dixon method to quantify intracellular lipid content in renal tumours. 3D T1W VIBE Dixon data were used to reconstruct a 3D fat fraction map of the entire RCC. The mean values of the fat fraction and SI_{index} were significantly higher in clear-cell than those in non-clear-cell RCCs. At the fat fraction cut-off value of 8.9% and SI_{index} cut-off value of 8.89%, sensitivities of 75% and 85.7%, specificities of 76.5% and 70.6%, were obtained, respectively for differentiating clear-cell from non-clear-cell RCC. The present findings differed from the previous report of the SI drop on out-of-phase CSI in angiomyolipoma and all subtypes of RCCs without significant association with pathology.[9] Excluding angiomyolipomas, the previous investigators found a >25% SI drop on CSI to be diagnostic for clear-cell RCCs; however, only areas with a visual SI drop, which reflected tumour cells with highest fat content rather than total fat content within the entire tumour, were measured. In renal masses with no macroscopically visible fat, a >20% SI drop was reported to be 57.5% sensitive and 96.5% specific with 92% positive predictive value whereas a >29% SI drop was 40% sensitive and 100% specific for differentiating clear-cell RCC from minimal-fat angiomyolipoma and non-clear-cell RCC[10]; however, the placement of ROIs was not described in the report. In the present study, areas of cystic degeneration, necrosis, and haemorrhage were not included in the ROIs. The mean ROI value of five MRI sections was calculated to minimise ROI selection bias and more accurately quantify the intracellular lipid content of different subtypes of RCC.

Most of the previous studies used conventional 2D CSI to evaluate intracytoplasmic lipid in renal masses.[6,9–11] The 2D technique is limited by ambiguity of fat or water dominance, exhibiting greatest signal loss at a 50% mixture of fat and water and thereby underestimating high lipid content.[16] By using both magnitude and phase information in the present study, the fat fraction calculated with the fat/water datasets in 3D Dixon sequence resolves the fat–water signal dominance ambiguity. The 3D Dixon technique has greater signal-to-noise ratio, which enables acquisition of thinner sections with no intersection gap. This improves spatial resolution along the *z*-axis, minimises the effect of partial volume averaging at the edge of the mass, and results in more accurate SI measurements.

Recent years, multiparametric MRI with CSI, T2W, DWI, and dynamic-contrast enhanced imaging to characterise renal tumours is now performed in clinical practice.[17–20] Cornelis *et al.*[18] took a multiparametric approach, analysing T2W, contrast-enhanced, DWI, and SI_{index} based on CSI sequences MRI findings in 100 renal cortical tumours. Their study indicated that different MRI sequences have different discrimination abilities for different tumour subtypes. Hotker *et al.*[20] took a multiparametric approach, using a combination of ADC, peak enhancement, and

downslope. As indicated in their study, a quantitative multiparametric MRI approach may yield greater discriminatory power in identifying clear-cell RCC than any of the single-parameter approaches. Their study found ADC values had the best diagnostic performance and CSI was of little value in the differentiation of clear-cell RCC with other renal cortical tumours, but they used conventional 2D CSI to evaluate intracellular lipid in renal masses. The composition of the group of tumours may have influenced the results. For example, they included angiomyolipoma and oncocytoma in the group, which were reported in some studies to have overlap with ccRCC at CSI.[9,21] In the present study, the 3D Dixon technique was used to evaluate the intracellular lipid among renal masses. The 3D Dixon technique has greater signal-to-noise ratio and higher spatial resolution, which may result in more accurate SI measurements. Additional studies should be performed in the future with the addition of other functional MRI techniques, such as dynamic-contrast enhanced imaging, MR perfusion, and intravoxel incoherent motion (IVIM) MRI to evaluate the performance of quantitative multiparametric MRI approach in the differentiation of renal masses.

The present study was limited by a relatively small number of non-clear-cell RCCs. A larger study sample is required to validate the fat fraction cut-off value of 8.9% and SI_{index} cut-off value of 8.89% for differentiating clear-cell from non-clear-cell RCCs. Histopathological confirmation of the lipid content was not obtained of the entire tumour or comparison of matched ROIs between histopathology specimens and the 3D T1-weighted VIBE Dixon image slices. Although the two-point Dixon method is more accurate for evaluating lipid content than CSI used in previous studies, the Dixon method is affected by $T2^*$-induced dephasing. Areas of haemorrhage in the ROIs were excluded to diminish the $T2^*$ decay. Multi-echo, gradient-echo, or IDEAL (iterative decomposition of water and fat with echo asymmetry and least-squares estimation) allows simultaneous fat–water decomposition and $T2^*$ estimation. It may correct for $T2^*$ decay on CSI-based fat–water separation and more accurately reflect the lipid content in future studies.[22,23]

In conclusion, intracellular lipid content analysis of RCCs using reconstructed 3D VIBE Dixon MRI can be helpful in the differentiation of clear-cell and non-clear-cell RCC.

References

1. Reuter VE. The pathology of renal epithelial neoplasms. *Semin Oncol* 2006;**33**(5):534–43.
2. Fleming S, O'Donnell M. Surgical pathology of renal epithelial neoplasms: recent advances and current status. *Histopathology* 2000;**36**(3):195–202.
3. Cheville JC, Lohse CM, Zincke H, *et al*. Comparisons of outcome and prognostic features among histologic subtypes of renal cell carcinoma. *Am J Surg Pathol* 2003;**27**(5):612–24.
4. Schieda N, van der Pol CB, Moosavi B, *et al*. Intracellular lipid in papillary renal cell carcinoma (pRCC): T2 weighted (T2W) MRI and pathologic correlation. *Eur Radiol* 2015;**25**(7):2134–42.
5. Oliva MR, Glickman JN, Zou KH, *et al*. Renal cell carcinoma: t1 and t2 signal intensity characteristics of papillary and clear-cell types correlated with pathology. *AJR Am J Roentgenol* 2009;**192**(6):1524–30.
6. Outwater EK, Bhatia M, Siegelman ES, *et al*. Lipid in renal clear-cell carcinoma: detection on opposed-phase gradient-echo MR images. *Radiology* 1997;**205**(1):103–7.
7. Schoth F, Persigehl T, Palmowski M. Current role and future perspective of MRI for diagnosis and characterization of renal cell carcinoma. *Panminerva Med* 2010;**52**(4):307–18.
8. Ramamurthy NK, Moosavi B, McInnes MD, *et al*. Multiparametric MRI of solid renal masses: pearls and pitfalls. *Clin Radiol* 2015;**70**(3):304–16.
9. Karlo CA, Donati OF, Burger IA, *et al*. MR imaging of renal cortical tumours: qualitative and quantitative chemical shift imaging parameters. *Eur Radiol* 2013;**23**(6):1738–44.
10. Jhaveri KS, Elmi A, Hosseini-Nik H, *et al*. Predictive value of chemical-shift MRI in distinguishing clear-cell renal cell carcinoma from non-clear-cell renal cell carcinoma and minimal-fat angiomyolipoma. *AJR Am J Roentgenol* 2015;**205**(1):W79–86.
11. Ferré R, Cornelis F, Verkarre V, *et al*. Double-echo gradient chemical shift MR imaging fails to differentiate minimal fat renal angiomyolipomas from other homogeneous solid renal tumors. *Eur J Radiol* 2015;**84**(3):360–5.
12. Yoshimitsu K, Irie H, Tajima T, *et al*. MR imaging of renal cell carcinoma: its role in determining cell type. *Radiat Med* 2004;**22**(6):371–6.
13. Marin D, Dale BM, Bashir MR, *et al*. Effectiveness of a three-dimensional dual gradient echo two-point Dixon technique for the characterization of adrenal lesions at 3 Tesla. *Eur Radiol* 2012;**22**(1):259–68.
14. Fischer MA, Donati OF, Chuck N, *et al*. Two- versus three-dimensional dual gradient-echo MRI of the liver: a technical comparison. *Eur Radiol* 2013;**23**(2):408–16.
15. Marin D, Soher BJ, Dale BM, *et al*. Characterization of adrenal lesions: comparison of 2D and 3D dual gradient-echo MR imaging at 3 T—preliminary results. *Radiology* 2010;**254**(1):179–87.
16. Rosenkrantz AB, Raj S, Babb JS, *et al*. Comparison of 3D two-point Dixon and standard 2D dual-echo breath-hold sequences for detection and quantification of the fat content in renal angiomyolipoma. *Eur J Radiol* 2012;**81**(1):47–51.
17. Sasiwimonphan K, Takahashi N, Leibovich BC, *et al*. Small (<4 cm) renal mass: differentiation of angiomyolipoma without visible fat from renal cell carcinoma utilizing MR imaging. *Radiology* 2012;**263**:160–8.
18. Cornelis F, Tricaud E, Lasserre AS, *et al*. Routinely performed multiparametric magnetic resonance imaging helps to differentiate common subtypes of renal tumours. *Eur Radiol* 2014;**24**:1068–80.
19. Cornelis F, Lasserre AS, Tourdias T, *et al*. Combined late gadolinium-enhanced and double-echo chemical-shift MRI help to differentiate renal oncocytomas with high central t2 signal intensity from renal cell carcinomas. *AJR Am J Roentgenol* 2013;**200**:830–8.
20. Hötker AM, Mazaheri Y, Wibmer A, *et al*. Differentiation of clear-cell renal cell carcinoma from other renal cortical tumors by use of a quantitative multiparametric MRI approach. *AJR Am J Roentgenol* 2017;**208**(3):W85–91.
21. Hindman N, Ngo L, Genega EM, *et al*. Angiomyolipoma with minimal fat: can it be differentiated from clear-cell renal cell carcinoma by using standard MR techniques? *Radiology* 2012;**265**:468–77.
22. Ma J, Song Z, Yan F. Detection of hepatic and pancreatic fat infiltration in type II diabetes mellitus patients with IDEAL-Quant using 3.0T MR: comparison with single-voxel proton spectroscopy. *Chin Med J (Engl)* 2014;**127**(20):3548–52.
23. Hofstetter LW, Yeo DT, Dixon WT, *et al*. Fat-referenced MR thermometry in the breast and prostate using IDEAL. *J Magn Reson Imaging* 2012;**36**(3):722–32.